Master equation approach to reversible and conservative discrete systems

Felipe Urbina and Sergio Rica
Facultad de Ingeniería y Ciencias and UAI Physics Center, Universidad Adolfo Ibáñez, Avenida Diagonal las Torres 2640, Peñalolén, Santiago, Chile
(Received 9 August 2016; published 28 December 2016)

A master equation approach is applied to a reversible and conservative cellular automaton model (Q2R). The Q2R model is a dynamical variation of the Ising model for ferromagnetism that possesses quite a rich and complex dynamics. The configuration space is composed of a huge number of cycles with exponentially long periods. Following Nicolis and Nicolis [G. Nicolis and C. Nicolis, Phys. Rev. A **38**, 427 (1988)], a coarse-graining approach is applied to the time series of the total magnetization, leading to a master equation that governs the macroscopic irreversible dynamics of the Q2R automata. The methodology is replicated for various lattice sizes. In the case of small systems, we show that the master equation leads to a tractable probability transfer matrix of moderate size, which provides a master equation for a coarse-grained probability distribution. The method is validated and some explicit examples are discussed.

DOI: 10.1103/PhysRevE.94.062140

I. INTRODUCTION

In statistical physics one basically considers a large set of reversible and conservative ordinary differential equations for the description of particle dynamics. The temporal evolution for this cumbersome problem, even for a modest number of particles, requires a statistical description that introduces the concept of a probability distribution function for the phase space of the system. Irreversibility, equilibrium, and, more importantly, nonequilibrium properties emerge from this probability conception of systems (with a large number of degrees of freedom) and its deterministic evolution. Briefly, the methodology reduces (under some assumptions) to a kinetic description that displays an irreversible behavior to equilibrium observed in macroscopic systems. The assumptions for this approach are (i) macroscopically, a system is described by a finite set of observables, (ii) the robust instability of the microscopic motions, which is at the basis of the sensitivity to initial conditions and the ergodic assumption, and (iii) a *stosszahlansatz* that introduces explicitly a broken before-after symmetry for the evolution of the probability distribution.

Nicolis *et al.* [1,2] introduced a systematic coarse-graining approach for the treatment of the macroscopical variables. As a consequence, this coarse graining breaks naturally the past-future symmetry in time, leading to an irreversible master equation for a reduced probability distribution function of the system. In the current paper we apply this systematic approach to conservative and explicit reversible cellular automata. In particular, we consider the Q2R model, introduced by Vichniac [3], which is a cellular automaton that runs on a two-dimensional grid of finite size and is reversible in a physical sense, that is, not only is the automaton rule invertible, but the backward rule reads exactly the same as the forward one. Moreover, it was shown by Pomeau [4] that the Q2R automaton possesses a conserved energy like quantity.

The main reason to apply the coarse-graining approach to a cellular automaton instead of to a coupled system of ordinary differential equations is because a cellular automaton is a discrete model with Boolean entities as microscopic variables, thus, the system is numerically reversible and conservative. In consequence, Q2R seems to be a good benchmark to test the principles of statistical physics. However, the phase space is finite, hence the dynamical system only possesses fixed points and periodic orbits; therefore it cannot be ergodic, at least in the usual sense of continuous dynamics. Nevertheless, for large enough systems, the phase space becomes huge and the periodic orbits may be, as we show, exponentially long, thus, in practice, of infinite period. Further, if the initial state is random, the temporal behavior may be quite random and it possesses many properties of chaotic systems, such as sensitivity to initial conditions and mixing. For any purpose, the observation of a short periodic orbit is really improbable for large enough systems with random initial conditions. In general, there is a huge number of initial conditions that are almost ergodic.

By "almost ergodic" we mean that the original Q2R system is formally not ergodic, because it only possesses finite periodic orbits. Although finite, these periodic orbits may be exponentially long, so an arbitrary initial condition explores vastly the phase space, validating the equivalence of ensemble and temporal averages. Indeed, numerical studies confirm that the premises of statistical physics are valid, in particular, observables may be computed using standard methods of statistical physics. We will show that temporal averages of a macroscopic quantity provide the same information as the master equation for the coarse-grained distribution functions.

The study of the dynamics and properties of the Q2R model has had a long history. Soon after the seminal works of Vichniac [3] and Pomeau [4], Herrmann [5] implemented the Q2R algorithm to study the two-dimensional Ising model in the frame of the microcanonical ensemble. He studied the global magnetization, obtaining an excellent representation for the magnetization as a function of the initial conserved energy, displaying a coherent picture for the phase transition of the Ising model. Later, Herrmann *et al.* [6] studied numerically the probability to reach an infinitely long period for some energies. Moreover, if the energy is large enough, this probability tends to unity [6]. Next Takesue [7] focused on the possible realization of statistical mechanics for reversible cellular automata. His studies concerned explicitly all classes of rules in the one-dimensional case, the Q2R being only a special case. However, the Q2R model (90R in his terminology) is the analog of an ideal gas of particles with speeds $+1$ or -1, a system that cannot reach equilibrium in practice. However, it is

ergodic only in thermodynamical equilibrium. More recently, in Ref. [8], Goles and Rica studied numerically the irreversible behavior and the existence of a spontaneous transition from a noncoherent state to a coherent state.

The present article is organized as follows. The Q2R model, its main features, and findings are presented in Sec. II, which is subdivided as follows: We briefly report the numerical studies of Ref. [8] in Sec. II A; the phase-space properties, in particular some results on the distribution of periods of the dynamics, are reported in Sec. II B; the sensitivity to initial conditions is discussed in Sec. II C; and the scope of the paper is presented in Sec. II D. Section III introduces the notion of a master equation for the statistical description of the dynamics. In Sec. IV we provide some precise examples, where a coarse graining is realized, in order to get an adequate and tractable master equation. We provide an exhaustive validation of the technique and we discuss different coarse graining over the phase space. Finally, we summarize in Sec. V.

II. THE Q2R MODEL

For simplicity, we consider a regular two-dimensional lattice with $N = L^2$ nodes, in which each node is only seen by its four closest neighbors (the von Neumann neighborhood); we use periodic boundary conditions. Each node k possesses a discrete value x_k that may take a value $+1$ or -1. The Q2R model, introduced by Vichniac [3], is based upon the following two-step rule:

$$x_k^{t+1} = x_k^{t-1}\phi\left(\sum_{i\in V_k} x_i^t\right),$$

where the function ϕ is such that $\phi(s=0) = -1$ and $\phi(s) = +1$ if $s \neq 0$. In the sum V_k denotes the von Neumann neighbor of the site k. The reversibility follows directly from the inverse relation $x_k^{t-1} = x_k^{t+1}\phi(\sum_{i\in V_k} x_i^t)$, which is the backward rule [notice that $\phi(\sum_{i\in V_k} x_i^t)^2 = 1$ in all cases].

This two-step rule may be naturally rewritten as a one-step rule by introducing a second dynamical variable [4]

$$y_k^{t+1} = x_k^t, \quad x_k^{t+1} = y_k^t\phi\left(\sum_{i\in V_k} x_i^t\right). \tag{1}$$

The rule (1) is complemented with the initial condition $x_k^{t=0}$ and $y_k^{t=0}$.

As shown by Pomeau [4], the energy

$$E[\{x^t, y^t\}] = -\frac{1}{2}\sum_{\langle i,k\rangle} x_k^t y_i^t \tag{2}$$

is conserved, $E[\{x^t, y^t\}] = E[\{x^{t=0}, y^{t=0}\}]$, under the dynamics defined by the Q2R rule (1). Moreover, the energy is bounded by $-2N \leqslant E \leqslant 2N$.

Despite the existence of an energylike quantity, it is not possible to speak about a Hamiltonian for a discrete dynamics because the variables x^t and y^t and the energy (2) are discrete quantities [4]. Moreover, supported by the existence of a large number of periodic orbits, it is believed that Q2R possesses a large number of other invariants. An example of additional conserved quantities are the staggered invariants [9]. Indeed, for a square periodic lattice of even size L ($N = L^2$), the full lattice may be divided into two sublattices as follows. We denote by k_x and k_y the indices of the full square. Then we define the W sublattice by all points such that $k_x + k_y$ is an even number, while the B lattice is characterized by the condition $k_x + k_y$ being an odd number. (In other words, these sublattices represent the white and black fields in the chessboard.) Then we define

$$E^W[\{x^t, y^t\}] = -\frac{1}{2}\sum_{k_x+k_y \text{ even}} x_k^t \sum_{i\in V_k} y_i^t,$$

$$E^B[\{x^t, y^t\}] = -\frac{1}{2}\sum_{k_x+k_y \text{ odd}} x_k^t \sum_{i\in V_k} y_i^t.$$

The conserved energy (2) may be rewritten as $E[\{x^t, y^t\}] = E^W[\{x^t, y^t\}] + E^B[\{x^t, y^t\}]$. Further,

$$J[\{x^t, y^t\}] = (-1)^t(E^W[\{x^t, y^t\}] - E^B[\{x^t, y^t\}]) \tag{3}$$

is also an invariant, i.e., $J[\{x^t, y^t\}] = J[\{x^{t=0}, y^{t=0}\}]$. This extra invariant splits the subspace of constant E into a subset of constant E and constant J. The role of this staggered invariant in the macroscopic behavior will be not be investigated in the present work.

A. Long-time dynamics of the Q2R cellular automata

Numerical simulations of the Q2R model in two space dimensions and for large system sizes, e.g., $N = 256 \times 256$, and random initial conditions show that the dynamics displays a fluctuating spatiotemporal pattern showing regions with states $+1$ and sectors with states -1, as well as zones with chessboardlike patterns [8]. The full patterns will be characterized by the global magnetization

$$M(t) = M[\{x^t\}] = \sum_k x_k^t. \tag{4}$$

Naturally, the function M is restricted to the set $\{-N, -N+2, \ldots, N-2, N\}$, therefore there are $N+1$ possible states of magnetization.

A detailed characterization of the evolution, as well as the fluctuations, for the magnetization has been treated in detail in Ref. [8]. Briefly, after a transient the average magnetization depends mainly on the initial energy. If the energy is low, one sees that the average magnetization evolves slowly in time to an equilibrium state with an almost constant value plus weak fluctuations. For larger energies, the fluctuations play an important role. One may observe that the system is in an almost stable state, but then suddenly jumps into a metastable state with zero average magnetization, and then jumps into an opposite magnetization state [8].

The plot of the temporal average for the global magnetization versus the energy is reported in Fig. 1. One can see that the magnetization spontaneously increases below a critical energy per site around $E_c/N = -1.4$, which is close to the critical energy of the Ising model $E_c/N = -\sqrt{2}$ [10,11]. Moreover, in Refs. [5,8] the magnetization is compared as a function of the internal energy of the system, showing a close agreement with numerical values.

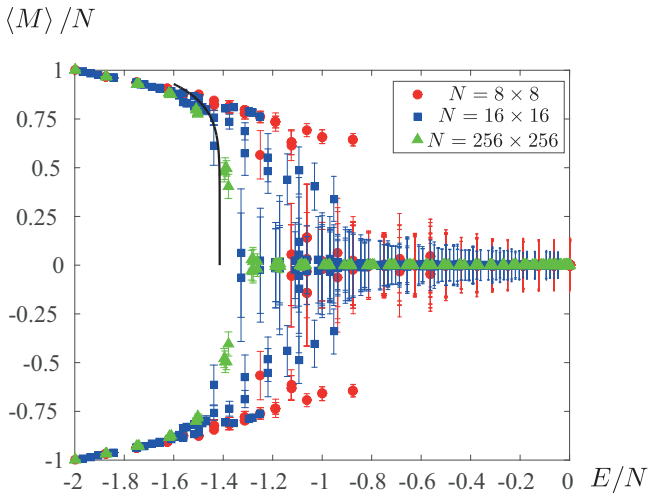

FIG. 1. Magnetization curves as a function of initial energy for three different system sizes $N = 8 \times 8$, $N = 16 \times 16$, and $N = 256 \times 256$, as indicated in the legend. Each point corresponds to a different initial condition; in this case we sample different energies. As it can be noticed, there is a finite system dependence on the critical behavior of the system. Indeed, the critical behavior disappears for small system sizes $N = 8 \times 8$ and $N = 16 \times 16$, whereas for large systems the magnetization curve reaches a critical behavior. The continuous line represents the well known statistical mechanics calculation for the Ising model $M/N \approx 2^{5/16}(\sqrt{2} + E/N)^{1/8}$.

We emphasize that the main feature of the Q2R automaton is that it shows a deterministic microcanonical dynamics. Moreover, as shown in Fig. 1, for larger size systems, the results agree with the thermodynamical calculations in an infinite system size [10,11]. On the other hand, other probabilistic evolutions, such as Monte Carlo simulations or Glauber dynamics [12], deal with a spin system in contact with a thermal bath, that is, in canonical equilibrium. However, as expected, both methodologies share the same macroscopic equilibrium.

B. Phase space

The configuration space of all states is defined through all possible values of the state $\{x, y\}$. The resulting space is composed of the 2^{2N} vertices of a $2N$-dimensional hypercube. The smallest possible system corresponds to an $N = 2 \times 2$ lattice. In this case there are $2^{2\times4} = 2^8 = 256$ states and the phase space is a hypercube in dimension 8. However, the dynamics is too simple; it contains cycles of period 4 at most. The phase space for a 4×4 system is the largest possible one that can be studied exactly, case by case. In this case the system possesses $2^{2\times16} = 2^{32}$ states and it contains a rich variety of cycles [13]. This case will be studied deeply as a good benchmark for conjectures in larger-dimensional systems.

As an example, from this case, it is observed that the total number of cycles $n(T, E)$ of period T and energy E would be bounded by [14]

$$n(T, E) < \frac{1}{T} 2^{2N} e^{-\alpha|E|} \sim e^{2N \ln 2 - \alpha|E|}.$$

From the data one has that for 3×3 and 4×4, $\alpha \approx 0.6$, but this value varies as the lattice size increases. Here one notices a dramatic difference among the cases depending on $|E|$ (greater or smaller than $E_c = \frac{2}{\alpha} \ln 2$). If $|E|$ is greater than E_c the probability to see a long period is exponentially small, but for $|E| < E_c$ this probability reaches unity. Higher lattice sizes confirm this scenario but modify slightly the value of α. This behavior is consistent with the numerical simulations of Ref. [6].

C. Sensitivity to initial conditions

The sensitivity to initial conditions of Q2R has been discussed previously in Ref. [8]. In fact, when starting from two distinct initial conditions, which share the same energy and J, they will evolve along two different paths. As the distance in phase space is bounded, these two cycles will diverge in a nonexponential way. However, the separation growth between them is fast enough so as to be completely analogous with the concept of sensitivity to initial conditions.

To perform this study we require two close enough initial configurations. A first initial configuration $\{x, y\}^{t=0}$ is arbitrarily chosen. The second one is built by swapping a single site $\bar{k}$ in the previous configuration. This site is randomly selected such that the average magnetization due to its neighbors is zero (that is $\sum_{i \in V_{\bar{k}}} x_i = 0$ or $\sum_{i \in V_{\bar{k}}} y_i = 0$). In this way, both initial configurations have the same energy. Finally, running independently both initial configurations, a separation distance between both paths can be measured by employing the so-called Hamming or Manhattan distance defined as

$$d_H(t) = \frac{1}{4N} \sum_{k=1}^{N} \left(\left| x_k^t - \bar{x}_k^t \right| + \left| y_k^t - \bar{y}_k^t \right| \right),$$

with $\{x, y\}^t$ and $\{\bar{x}, \bar{y}\}^t$ denoting two different sequences belonging to two different cycles. It can be shown numerically that $d_H(t)$ grows approximately as t^2 (see Ref. [8] for details).

D. Scope of the paper

Though the Q2R model is quite simple its dynamics is usually very rich, as it has been documented extensively in the literature. Moreover, this conservative and reversible system appears to behave as a typical macroscopic system, as the number of degrees of freedom increases, showing a typical irreversible behavior, sensitivity to initial conditions, a kind of mixing, etc. It is believed that this Q2R is a good representation of an Ising model in thermodynamical equilibrium.

The phase space of the Q2R system of N sites possesses 2^{2N} states, which are partitioned in different subspaces of constant energy, which are partitioned into a large number of smaller subspaces of periodic orbits or fixed points. Notice that, because the system is conservative, there are neither attractive nor repulsive limit sets; all orbits are fixed points or cycles.

This feature of the phase space is schematized in Fig. 2(a), where the constant energy subspace shares in principle many cycles and fixed points. An arbitrary initial condition of energy E falls into one of these cycles and runs until it returns to the initial configuration after a time T, which could

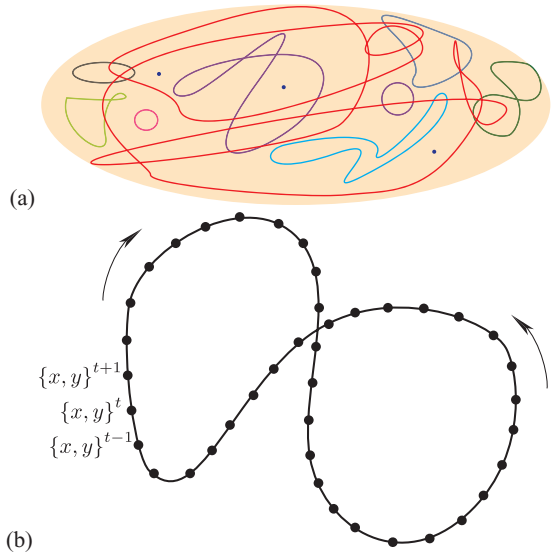

FIG. 2. (a) Scheme for a subspace of constant energy composed of a number of cycles and fixed points. (b) Cartoon of a cycle of period T, for which the cycle is composed of T states.

be exponentially long, and it displays a complex behavior (not chaotic, strictly speaking; see, for instance, [15]). More importantly, the probability that an initial condition exhibits such a complex behavior is finite [6]. Moreover, Q2R manifests sensitivity to initial conditions, that is, if one starts with two distinct, but close, initial conditions, then the conditions will evolve into very different cycles as time runs [8]. In some sense, an initial state explores vastly the phase space, justifying the grounds of statistical physics.

In conclusion, the overall picture is that, although for a finite-size system the deterministic automaton Q2R possesses periodic dynamics so it is not ergodic, there is a huge number of initial conditions that explore vastly the configuration space (this is particularly remarkable for initial conditions of random structure). Therefore, one expects that a master equation approach may be successful.

III. MASTER EQUATION

A. General formalism

Given a set of initial conditions with a fixed energy E, the probability distribution $\varrho_t^E(\{x,y\})$ evolves following a Perron-Frobenius-like equation

$$\varrho_{t+1}^E = \mathcal{L}^E \varrho_t^E, \tag{5}$$

which, in principle, can be computed by using the microscopic evolution rule (1). Indeed, $\mathcal{L}^E$ is easy to build: If the state $\{x,y\}_i$ at time t evolves into $\{x,y\}_k$ at time $t+1$, then one sets the (i,k) components equal to 1, that is, $\mathcal{L}_{ik}^E = 1$. Checking all available elements $\Omega(E)$ for a given energy, we can build the huge, $\Omega(E) \times \Omega(E)$, linear operator $\mathcal{L}^E$. This matrix possesses a large number of blocks and zeros, revealing the existence of a large number of cycles in the Q2R model (in some sense, $\mathcal{L}^E$ is a kind of adjacency matrix of a graph, the graph being the total number of existing cycles for a given energy). However, this description is impractical because of the typical magnitude of $\Omega(E)$. Therefore, the full phase space is reduced to a description using gross or macroscopic variables, namely, the total magnetization (4), instead of microscopic variables.

We proceed with a coarse-graining scheme as in Ref. [1]. Let us define a noninvertible projection operator Π that maps the original distribution function ϱ_t^E onto $\rho_t(M)$,

$$\rho_t(M) = \Pi \cdot \varrho_t^E(\{x,y\}) = \sum_{\text{states with } \sum_k x_k = M} \varrho_t^E.$$

Formally, ϱ_t^E may be seen as a vector of dimension $\Omega(E)$ and ρ_t as a vector of dimension $N+1$, indexed by M; hence Π is formally a matrix with $N+1$ rows and $\Omega(E)$ columns. Applying the projector operator on the Perron-Frobenius equation (5), one gets

$$\rho_t(M) = \Pi \cdot \varrho_t^E = \Pi \cdot \mathcal{L}^E \cdot \varrho_{t-1}^E = \Pi \cdot (\mathcal{L}^E)^t \cdot \varrho_0^E, \tag{6}$$

where $\varrho_0^E(\{x,y\})$ is an initial distribution.

As explained in detail in Ref. [1], in general, it is not possible to reduce the original Perron-Frobenius equation to a self-contained master equation. Following, Nicolis *et al.* [1,2], we take an initial reduced distribution $\varrho_0^E(\{x,y\})$ as a combination of step functions in the aforementioned intervals:

$$\varrho_0^E(\{x,y\}) = \sum_M \alpha_M \varphi_M(\{x,y\}). \tag{7}$$

In Eq. (7) we have defined

$$\varphi_M(\{x,y\}) = \begin{cases} 1 & \text{for } \sum_k x_k = M \\ 0 & \text{for } \sum_k x_k \neq M. \end{cases}$$

The linear operator φ may be seen as a matrix with $N+1$ rows and $\Omega(E)$ columns (a state $\{x,y\}$ that belongs to a column vector of dimension $\Omega(E)$ and maps onto a single magnetization, which may take $N+1$ different values). This is the central assumption of the coarse-graining approximation. States with the same magnetization are assumed to be uniformly distributed in the original phase space [see the ansatz (7)]. The coefficients α_M may be obtained by inverting (7) [1]. The result is

$$\alpha_M = \sum_{\text{states}} \varrho_0^E(\{x,y\}) \varphi_M(\{x,y\}).$$

Therefore, α_M is precisely the Mth component for the coarse-grained distribution $\rho_0(M) = \Pi \varrho_0^E$. Thus, for this special type of initial distribution one has

$$\varrho_0^E(\{x,y\}) = \sum_M \rho_0(M) \varphi_M(\{x,y\}) = \varphi^\dagger \cdot \boldsymbol{\rho}_0.$$

In the last equality we have written explicitly $\boldsymbol{\rho}_0$ as an $(N+1)$-dimensional vector and $\varphi^\dagger$ as an $\Omega(E) \times (N+1)$ matrix. Therefore, the Perron-Frobenius equation (6) becomes

$$\boldsymbol{\rho}_t = \Pi \cdot (\mathcal{L}^E)^t \cdot \varphi^\dagger \cdot \boldsymbol{\rho}_0. \tag{8}$$

Notice that $\varphi^\dagger \cdot \Pi = I$ is the $\Omega(E) \times \Omega(E)$ identity matrix. Therefore, defining the $(N+1) \times (N+1)$ matrix $\mathcal{W}$ by

$$\mathcal{W} = \Pi \cdot \mathcal{L}^E \cdot \varphi^\dagger, \tag{9}$$

one is able to write the final reduced Perron-Frobenius equation, which will be of the form

$$\boldsymbol{\rho}_{t+1} = \mathcal{W} \cdot \boldsymbol{\rho}_t. \tag{10}$$

The linear operator $\mathcal{W}$ acts only in the subspace of constant E, but is spanned over arbitrary values of magnetization, and at the same time the reduced density $\boldsymbol{\rho}$ is a vector with its components indexed by M.

As in the original Perron-Frobenius equation, $\mathcal{W}$ depends explicitly on the Q2R rule through $\mathcal{L}^E$; therefore, in principle, it is possible to compute it explicitly. However, in practice, because of the complex and unknown structure of $\mathcal{L}^E$ (in particular because of the existence of a myriad of different periods for a given E), it is not a realistic task because the matrix $\mathcal{W}$ could be quite large.

However, the matrix $\mathcal{W}$ can be further reduced following a second coarse-graining process. This partition is defined through a finite number of sets of nonoverlapping intervals $I_1 = [-N, M_1), I_2 = [M_1, M_2), \ldots, I_{K-1} = [M_{K-2}, M_{K-1}), I_K = [M_{K-1}, N]$. [The previous case (10) corresponds to $K = N + 1$.]

We can proceed as previously, defining a second noninvertible projection operator π that maps the reduced distribution function ρ_t into a discrete and shorter column vector of dimension K: $\boldsymbol{f}_t = (f_1, f_2, \ldots, f_K)$. Finally, we obtain a coarse-grained master equation for the probability distribution [1,2]

$$\boldsymbol{f}_{t+1} = \hat{W} \cdot \boldsymbol{f}_t. \tag{11}$$

Here $\hat{W}$ is named the transition probability matrix.

The following are important features of the master equation (11).

(i) The probability vector $\boldsymbol{f}_t$ should be positive and normalizable. Let $\mathbf{1} = (1, 1, \ldots 1)$ be a K-dimensional vector; then we set $\mathbf{1} \cdot \boldsymbol{f}_t = 1$. More importantly, because of normalization $\sum_{i=1}^{K} w_{ik} = 1$, one has $\hat{W}^\dagger \cdot \mathbf{1} = \mathbf{1}$. This implies that the probability is conserved under the evolution $\mathbf{1} \cdot \boldsymbol{f}_{t+1} = \mathbf{1} \cdot \hat{W} \boldsymbol{f}_t = \mathbf{1} \cdot \boldsymbol{f}_t = 1$.

(ii) The Perron-Frobenius equation could be solved exactly provided it is given an initial given distribution $\boldsymbol{f}_0$: $\boldsymbol{f}_t = \hat{W}^t \boldsymbol{f}_0$.

(iii) Because of the Frobenius theorem, there exists an eigenvalue that is one, $\lambda_1 = 1$, while other eigenvalues fall inside the unitary circle $|\lambda_i| < 1$ for $i > 1$. Let $\boldsymbol{f}_{\text{eq}}$ be the eigenvector associated with the eigenvalue $\lambda_1 = 1$; this is an invariant vector $\boldsymbol{f}_{\text{eq}} = \hat{W} \boldsymbol{f}_{\text{eq}}$.

(iv) In what it follows we denote by $\boldsymbol{\chi}^{(i)}$ the eigenvectors of $\hat{W}$ corresponding to λ_i. Naturally one has $\boldsymbol{\chi}^{(1)} \equiv \boldsymbol{f}_{\text{eq}}$.

(v) There exists an equilibrium state $\lim_{t\to\infty} \boldsymbol{f}_t = \boldsymbol{f}_{\text{eq}}$.

(vi) Because all elements in the W matrix are positive, any non-negative initial distribution remains non-negative.

B. Explicit calculation for the transition probability matrix $\hat{W}$

As already mentioned, to determine empirically the matrix $\mathcal{W}$ or $\hat{W}$, we cannot use (9). Instead, we start with a magnetization sequence $\{\ldots, M_{t-1}, M_t, M_{t+1}, \ldots\}$ obtained from direct numerical simulations. This sequence is always finite, but it could be exponentially long (so in practice infinite).

The transition probability matrix $\hat{W}$ may be found from the probability density functions at times t and $t + 1$. The elements of the matrix are given by the following conditional probabilities (here we use different notation than in Ref. [1]):

$$w_{ik} = P(M_{t+1} \in I_i | M_t \in I_k) = \frac{P(M_{t+1} \in I_i \cap M_t \in I_k)}{P(M_t \in I_k)}.$$

Here M_t belongs to the interval I_k at time t and M_{t+1} belongs to the interval I_i at $t + 1$. Finally, the matrix $\hat{W}$ does not depend on time, which is a feature of a Markov process. The coarse-graining method is schematized in Fig. 3.

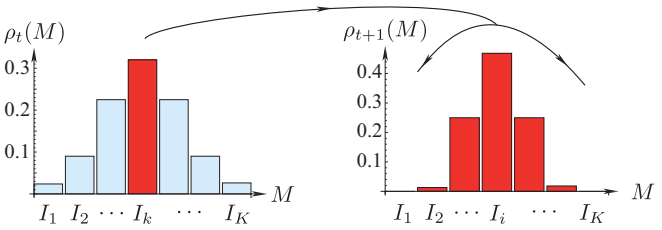

FIG. 3. Distribution $\rho_t(M)$ at a time t schematized in the distribution on the left. The fraction inside the interval I_k is distributed after the evolution into a new distribution $\rho_{t+1}(M)$ schematized in the diagram on the right. The normalized distribution provides the kth element of the ith column: w_{ik}.

C. Chapman-Kolmogorov condition and time-reversal symmetry

The final expression for the probability transition matrix (9) found after applying the formalism of Refs. [1,2] follows directly from Eq. (8) and the ansatz (7), which implies $\varphi^\dagger \cdot \Pi = I$. These relations are equivalent to the so-called compatibility condition

$$\Pi \cdot (\mathcal{L}^E)^t \cdot \varphi^\dagger = \mathcal{W}^t.$$

This compatibility condition (or Chapman-Kolmogorov condition) arises as a result of the approximations done in Sec. III A, however it is not a general property of the dynamics. For instance, by taking a complete cycle ($t = T$), one readily gets

$$\Pi \cdot (\mathcal{L}^E)^T \cdot \varphi^\dagger = I$$

(with I being the identity matrix), which evidently differs from $\mathcal{W}^T$ because $\mathcal{W}$ represents an irreversible behavior toward equilibrium. Therefore, the compatibility condition is only valid as an approximation for a limited number of time steps that enter to a particular sequence. The same argument holds for the reduced matrix $\hat{W}$ defined through (11).

Let us call $\hat{W}^{(\tau)}$ the resulting probability transfer matrix after τ steps; that is, by computing $\hat{W}$ as a consequence of the evolution from t up to $t + \tau$, the Chapman-Kolmogorov or compatibility condition for $\hat{W}$ reads

$$\hat{W}^{(\tau)} = \hat{W}^{(\tau_1)} \cdot \hat{W}^{(\tau_2)}, \tag{12}$$

where $\tau = \tau_1 + \tau_2$. In particular, for $\tau_1 = \tau_2 = 1$ one should satisfy

$$\hat{W}^{(2)} = \hat{W} \cdot \hat{W} = \hat{W}^2.$$

Other compatibility conditions are

$$\hat{W}^{(3)} = \hat{W}^{(2)} \cdot \hat{W}, \quad \hat{W}^{(3)} = \hat{W} \cdot \hat{W}^{(2)},$$

$$\hat{W}^{(4)} = \hat{W}^{(2)} \cdot \hat{W}^{(2)}, \quad \hat{W}^{(4)} = \hat{W} \cdot \hat{W}^{(2)} \cdot \hat{W},$$

etc. In Sec. IV C we check in practice how well these Chapman-Kolmogorov conditions are satisfied.

Finally, let us state an important result due to Pomeau [16]. The K-time correlation functions impose some restrictions on the W matrix. Because of time-reversal symmetry, for all indices $i_1, i_2, \ldots, i_K = \{1,2,\ldots,K\}$ the symmetry relation

$$w_{i_1 i_2} w_{i_2 i_3} \cdots w_{i_{K-1} i_K} w_{i_K i_1} = w_{i_1 i_K} w_{i_K i_{K-1}} \cdots w_{i_3 i_2} w_{i_2 i_1} \quad (13)$$

must be satisfied. In what it follows, we apply this coarse-graining approach to compute the probability transfer matrix for some particular cases.

IV. SPECIFIC COMPUTATION OF THE TRANSITION PROBABILITY MATRIX IN VARIOUS SITUATIONS

In this section we apply the coarse-graining approach to the Q2R dynamics in the case of a small lattice size. In Ref. [17] we have explored the computation of the transition probability matrix, in particular, in the case of extended systems ($N = 256 \times 256$). However, in this case the cycles are usually huge, therefore this general approach is not really satisfactory. In this sense, we focus our effort on treating systems of moderate sizes, namely, $N = 4 \times 4$, $N = 8 \times 8$, and $N = 16 \times 16$, all of them having tractable cycles.

A. Robustness of the methodology

In general, for a system of small size, one is able to find some cycles for a given energy. Building a time series for the magnetization $\{M(t)\} = \{M_1, M_2, \ldots, M_T\}$, one defines a partition of the possible values of the magnetization, as explained in Sec. III. In the cases considered here, it is always possible to use the finest possible partition, that is, for the exact available values of the magnetization (something impractical in large systems). In this case the partitions are composed of a set of $N+1$ (N is assumed to be even) well defined values $M = \{-N, -N+2, -N+4, \ldots, N-2, N\}$. That is, for 4×4 the partition has a maximum of 17 elements, for $N = 8 \times 8$ there are 65 elements, and for $N = 16 \times 16$ the partition possesses a maximum of 257 elements.

The first result concerns the equivalence of the probability density function of magnetization obtained via the time series of the magnetization and the equilibrium distribution resulting from the eigenvectors of the transition probability matrix $\hat{W}$. Hence, the results arising from temporal averages and the transition probability matrix in the configuration space are consistent among themselves. This fact ensures an initial validation of the method. However, the transition probability matrix provides extra information about a system, including the nonequilibrium properties, given by the spectrum of $\hat{W}$.

Next we describe the methodology for the case of a lattice of size 16×16 for an orbit with $E = -292$ and period $T = 43\,115\,258$. The transition probability matrix $\hat{W}$ is constructed following the steps of Sec. III B. However, first we verify that the master equation does not strongly depend on the length of the time series for the magnetization. It is important to remark that we think that this is a crucial step, because it allows us to compare explicitly the dependence of the results on the partial length of the cycles, something that is not possible for larger systems, because in these cases we would never be able to build the complete period for the time series.

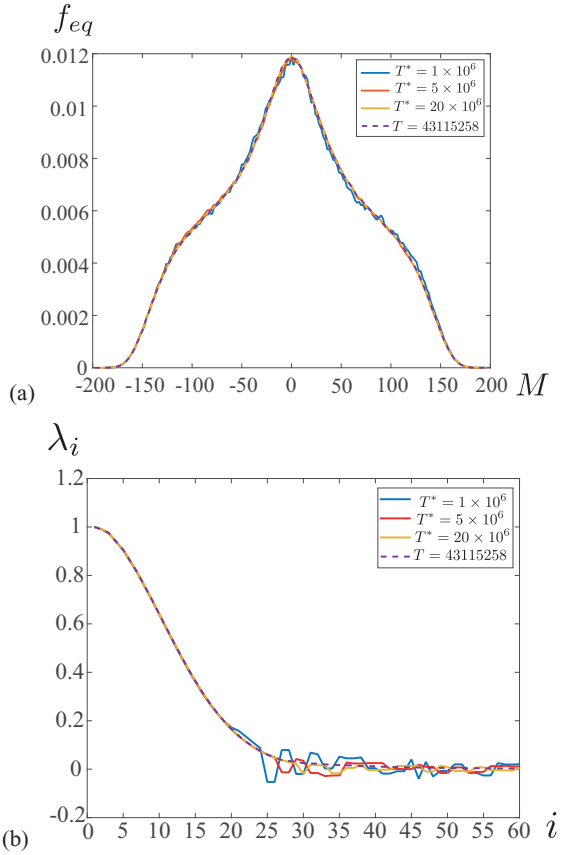

FIG. 4. (a) Plot of the equilibrium distribution $\boldsymbol{f}_{\text{eq}}$ for the case of a 16×16 system size with $E = -292$ ($E/N \approx -1.14$) and a cycle of period $T = 43\,115\,258$ (the complete cycle). The computation of $\boldsymbol{f}_{\text{eq}}$ is compared with shorter sequences of the same time series of length $T^* = 10^6, 5 \times 10^6, 20 \times 10^6$. (b) Set of 257 eigenvalues of the $\hat{W}$ matrix for the same conditions as in (b).

To test the above, we use again the finest partition. In this case, the transition matrix is of dimension 257×257 (so we will not provide it explicitly) and we characterize it by its equilibrium distribution and the full set of eigenvalues of $\hat{W}$. Figure 4(a) plots the equilibrium distributions $\boldsymbol{f}_{\text{eq}}$ for the total cycle T and $\boldsymbol{f}^{T^*}$ for the partial cycle of length T^*. Similarly, Fig. 4(b) plots the set of 257 eigenvalues, denoted by $\lambda_i^{T^*}$, for the same sequence $\{M(t)\}$, but for four different lengths of the time series. Visually, no substantial difference among the different values of T^* can be observed. Moreover, Table I compares quantitatively the mean square difference measuring $Q_1 = ||\boldsymbol{f}^{T^*} - \boldsymbol{f}_{\text{eq}}||^2/K$ and $Q_2 = \sum_{i=1}^{K} |\lambda_i - \lambda_i^{T^*}|^2/K$. Here K is the number of partitions.

TABLE I. Error estimation of the equilibrium distribution and the spectral decomposition of the $\hat{W}$ matrix for different lengths of the time series.

$T*$	Q_1	Q_2
10^6	3.95×10^{-5}	0.0038
5×10^6	3.91×10^{-5}	0.0020
20×10^6	3.84×10^{-5}	0.0002

Notice that an important feature of the transition probability matrix is that its eigenvalues are real if the time series satisfies reversibility [16]. We have verified that the coarse-graining approach applied to the full cycle with period T shows this important feature. Namely, the eigenvalues of the $\hat{W}$ matrix are real numbers. However, as we apply the same approach to a partial sequence of the same cycle of length less than T, some eigenvalues become complex (typically located near the origin in the complex plane). This is important because, in practice, for larger-size systems, one never closes a cycle, hence only incomplete sequences are available and thus the matrix would not have, in general, pure real eigenvalues. However, we emphasize that the existence of these complex eigenvalues is spurious.

Finally, it is important to compare results for partitions of different size. First, we compute the equilibrium distribution for three different partitions sets, more precisely, for an 8×8 system evolving by Q2R at $E = 0$ in a periodic orbit of $T = 672\,018$. Figure 5(a) compares the three different coarse-graining partitions (containing 5, 11, and 34 elements). Despite the evident differences among the coarse- and the finer-graining partitions, one notices that both partitions exhibit the same accurate behavior of the equilibrium distribution.

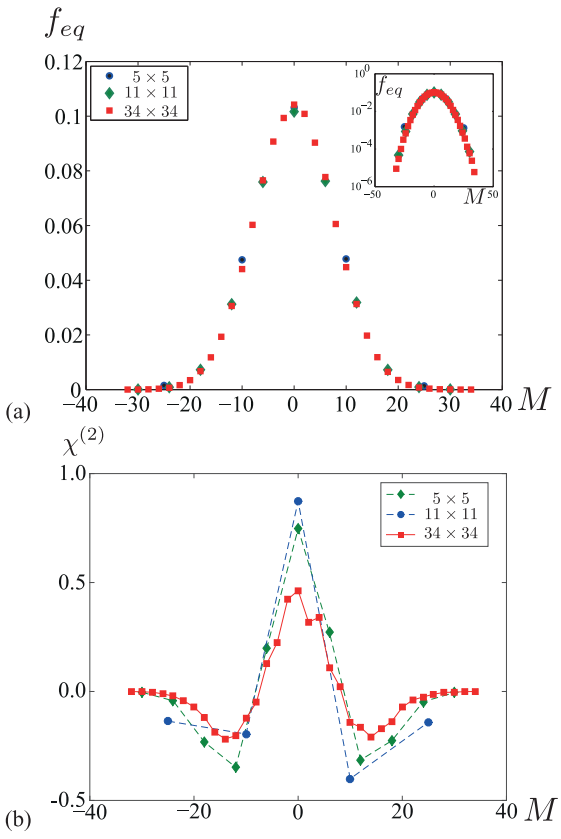

FIG. 5. (a) Plot of the equilibrium distribution $f_{\rm eq}$ vs M for an 8×8 system size with $E = 0$ and a cycle of a period $T = 672\,018$ for three different partitions of the magnetization values. The plot shows how all distribution functions lie under the same curve. The inset shows the parabolic behavior in magnetization, which after a fit reads $\ln f_{\rm eq} = -M^2/116$. (b) Plot of the second eigenmode $\boldsymbol{\chi}^{(2)}$ corresponding to the eigenvalue closest to the unit circle. It is noticeable how all partitions produce similar results.

Moreover, Fig. 5(b) compares the second eigenmode $\boldsymbol{\chi}^{(2)}$ without any substantial difference among the partitions.

In what follows, we summarize the methodology for cases of sizes 4×4, 8×8, and 16×16. In all cases, the full cycles are considered and we provide the finest possible partition.

B. Exact calculation for various lattices

We have studied in detail the case of a 4×4 periodic lattice because the phase space possesses $2^{32} \approx 4 \times 10^9$ distinct configurations and the calculations can be completely performed, thus showing explicitly the method. It is shown that the coarse-graining approach is fully applicable in the 4×4 lattice case. We used different partitions, getting a well defined probability transfer matrix $\hat{W}$. Reference [13] summarizes the calculations and main characteristics for various energies.

Next we explore a few cycles for larger systems (8×8 and 16×16). The cycles in these cases may be as long as desired for any practical purpose so that the equilibrium distribution is calculated with enough precision.

In the case of 8×8, for various energies and the finest possible coarse graining, for the sake of brevity, we omit explicitly the plots of the first eigenvector $\boldsymbol{f}_{\rm eq}$ as well as the eigenvalues because they are similar to the 16×16 lattice case.

The case of a 16×16 system size displays the most accurate equilibrium distribution found in the current research. The fluctuations around the distribution are small and the eigenvalues seem to form a continuous spectrum (the difference between two consecutive eigenvalues is small). We have also explored a wide range of energies. The rank of the matrices (that is, for the finest partition) is $K = 122$ for $E = -332$, $K = 205$ for $E = -316$, $K = 197$ for $E = -292$, $K = 129$ for $E = -168$, and $K = 101$ for $E = -92$. The equilibrium distribution, as a function of the magnetization, is plotted in Fig. 6(a). Similarly, the spectral decomposition is shown in Fig. 6(b).

In Fig. 6(a) one notices how in the case of larger energies, say, $E = -92$ and -168, the equilibrium distribution function is symmetric, under the change $M \to -M$; however, as the energy decreases one sees that for the lowest energy $E = -332$ a spontaneous symmetry breaking appears, so the equilibrium distribution is no longer an even function. The equilibrium probability may manifest a positive or negative magnetization (switching from one case to the other by changing the initial condition via the transformation $\{x, y\}^{t=0} \to \{-x, -y\}^{t=0}$). Moreover, the energy $E = -316$ case shows an equilibrium probability density function that manifests bi-stability. Indeed, these bimodal distributions possess three peaks, one at $M = 0$ and the two other at $M = \pm M_0 \neq 0$. Finally, the width of the probability density functions increases near the transition energy.

Figure 6(b) shows the spectral distribution of the probability transfer matrix that defines the master equation. Already for a lattice of size 16×16 one observes how the spectral distribution is almost continuous. One notices that the energies $E = -316$ and -292 possess the largest eigenvalues for a given index i. This means that, probably, the largest eigenvalues occur near the critical energy.

It is interesting to remark that the nonequilibrium is governed by those eigenvalues close to one. The nonequilibrium features behave as slow modes. In the current case one has

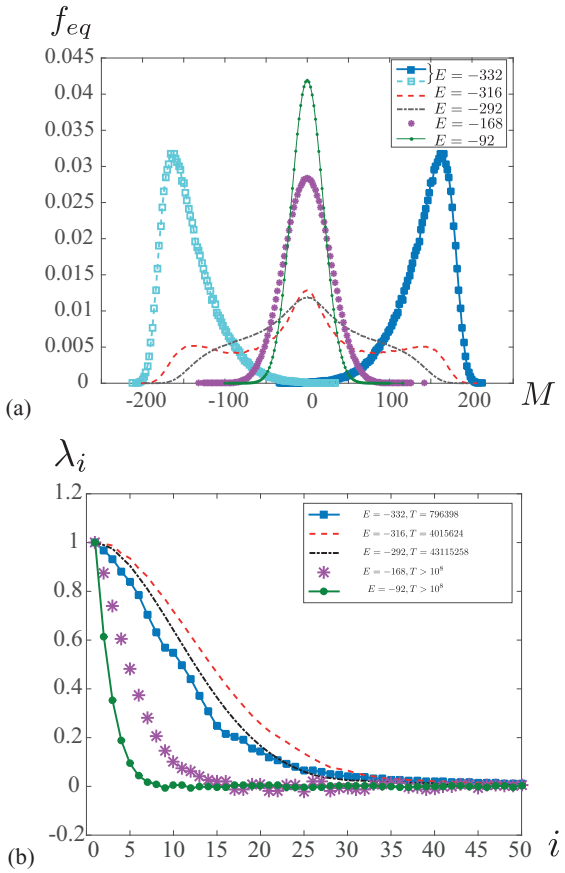

FIG. 6. (a) Equilibrium distributions $\boldsymbol{f}_{\text{eq}}$ for the case of a 16×16 system size and for the energies and periods $E = -332$ and $T = 796\,398$, $E = -316$ and $T = 4\,015\,624$, and $E = -292$ and $T = 43\,115\,258$, respectively. We also consider $E = -168$ and -92 with periods larger than $T > 10^8$. (b) Eigenvalues of the W matrix showing the existence of long-wave relaxation properties.

$\boldsymbol{f}_t = \sum_{i=1}^{K} \alpha_i \lambda_i^t \boldsymbol{\chi}^{(i)}$. Defining $\sigma_i = -\ln \lambda_i$, one obtains the usual slow mode relaxation. Moreover, the global behavior of the eigenvalues closest to unity represents the transport coefficients [17]. Figure 6(b) indicates that $\lambda_i \approx 1 - \gamma i$, which suggests that the nonequilibrium features are governed by a Fokker-Planck kind of equation. The behavior of the eigenvector agrees also qualitatively with this picture (see [17] for more details).

C. Chapman-Kolmogorov conditions

We have checked the Chapman-Kolmogorov relations for the case of Q2R in a 16×16 lattice for the case of $E = -292$ and a periodic orbit of $T = 43\,115\,258$. We have built five different probability transfer matrices $\hat{W}^{(\tau=1)}, \ldots, \hat{W}^{(\tau=5)}$ (see Sec. III C for the definition of $\hat{W}^{(\tau)}$).

First, we compared the matrices $\hat{W}^{(\tau=2)}$ and $\hat{W}^{(\tau=1)} \cdot \hat{W}^{(\tau=1)}$, both of rank 197×197, computing the distance between them, e.g., $\hat{W}^{(\tau=2)}$ and $\hat{W}^{(\tau=1)} \cdot \hat{W}^{(\tau=1)}$, via the usual distance (the square indicates the product of a matrix by itself)

$$d = \frac{1}{K^2} \text{Tr}[(\hat{W}^{(\tau=2)} - \hat{W}^{(\tau=1)} \cdot \hat{W}^{(\tau=1)})^2].$$

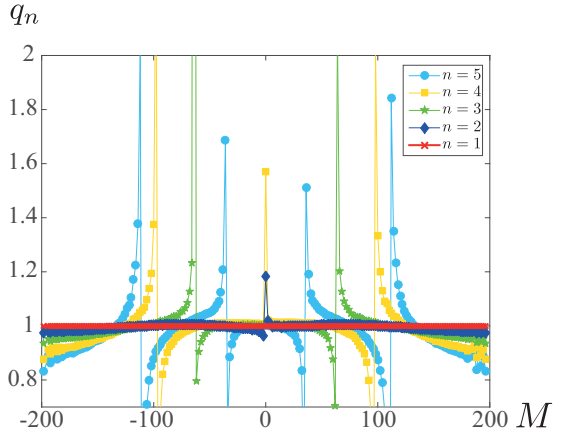

FIG. 7. Plot of the ratio q_n for five eigenmodes for the case of a 16×16 system.

In the current case, the matrices are similar up to $d = 5.81 \times 10^{-6}$. More quantitatively, we look at how good the eigenvectors of different matrices are, namely, $\hat{W}^{(\tau=2)}$ and $\hat{W}^{(\tau=1)} \cdot \hat{W}^{(\tau=1)}$. To do that, we compute the ratio among the nth eigenvectors of the aforementioned matrices, that is,

$$q_n = \frac{\chi_n^{(2)}}{\chi_n^{(1)}},$$

where $\chi_n^{(2)}$ and $\chi_n^{(1)}$ are the nth eigenvector of the matrices $\hat{W}^{(\tau=2)}$ and $\hat{W}^{(\tau=1)}$. This quantity is plotted in Fig. 7. One notices that $q_n \approx 1$ almost for all values of magnetization, but it also has an anomalous behavior near the nodal points of the eigenvector $\chi_n^{(1)}$. In general, the agreement of all these eigenvectors is satisfactory.

Next we check the Chapman-Kolmogorov relations written in Sec. III C, comparing the spectral properties of both matrices, namely, the set of eigenvectors and its eigenvalues. As can be seen in Fig. 8(a), the equilibrium distribution $\boldsymbol{f}_{\text{eq}}$ matches perfectly for different values of $\tau = \{1,2,3,4,5\}$. This proves that the equilibrium configuration $\boldsymbol{f}_{\text{eq}}$ is an invariant of the dynamical system. However, nonequilibrium properties do depend on the sampling time τ. Indeed, the eigenvalues corresponding to different probability transfer matrices do depend on the choice of the parameter τ. This is not a surprise, because it is expected that the eigenvalues $\lambda_i^{(\tau)}$ of $\hat{W}^{(\tau)}$ should scale as $\lambda_i^{(\tau)} = \lambda_i^{\tau}$, where λ_i are the set of eigenvalues of $\hat{W}^{(\tau=1)}$. This scaling is shown in Fig. 8(b), indicating an anomaly because it does not work for the case $\tau = 1$, but the scaling works well for higher τ. This deserves more careful study.

D. Pomeau's reversal symmetry relation

According to Pomeau [16], the microscopic time-reversal symmetry imposes the symmetry relation (13). For rank-K transition probability matrices, it is possible to verify that there are K^K different required conditions (13). Therefore, it is only possible to check this condition for a moderate rank K. For the case of 4×4 all probability transfer matrices that we have checked satisfy Pomeau's reversal symmetry relation [13]. For larger $\hat{W}$ matrices, say, $K > 9$, we have not

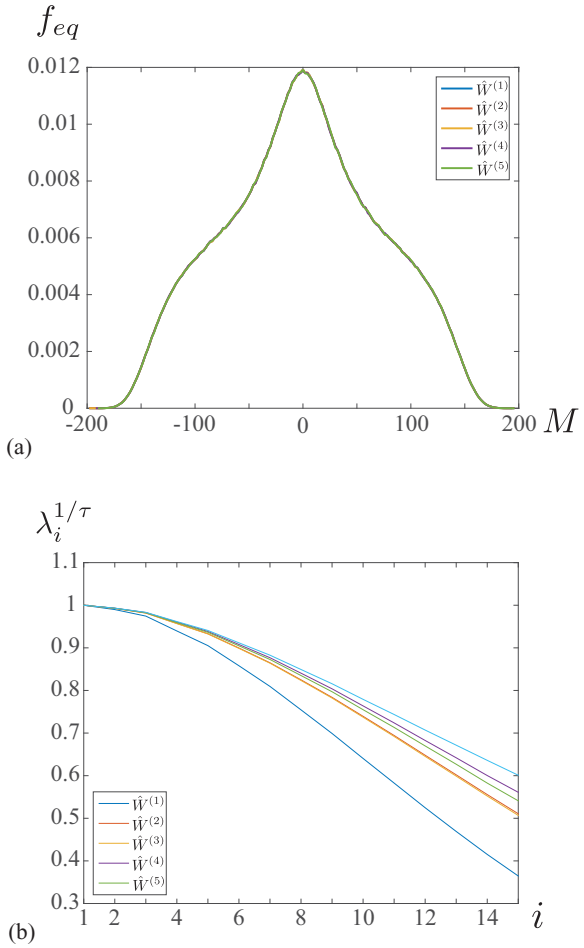

FIG. 8. (a) Equilibrium distributions $\boldsymbol{f}_{\text{eq}}$ for the case of a 16×16 system and for the energy $E = -292$ and $T = 43\,115\,258$. (b) Eigenvalues of the W matrix showing the existence of long-wave relaxation properties.

checked Pomeau's relation because it involves a cumbersome numerical calculation.

V. CONCLUSION

The basic properties of a Q2R cellular automaton, namely, its formal reversibility and the existence of a conserved energy, suggest that Q2R could be a good benchmark to test ideas of statistical mechanics. More importantly, the reversibility is not conditioned by any kind of approximate numerical algorithm. The Q2R model possesses a rich dynamics characterized by a huge number of invariants that partition the phase space in terms of the conserved energy and a huge number of periodic cycles. Although in a system of moderate size the periods are huge [6], for lattices of small size these cycles may be fully characterized.

We introduced a coarse-graining approach that allowed us to write a coarse-grained master equation, which characterizes equilibrium and nonequilibrium statistical properties of the system. We reviewed the methodology and tested the consistency of results in lattices of different sizes. We found that for well chosen partitions, this coarse-graining technique is a powerful tool to reduce the information of the whole system in such a way as to obtain a tractable probability transfer matrix that simplifies the original master equation. One central property of this matrix is the existence of an invariant probability distribution that agrees with different coarse-graining procedures. In addition, we computed the spectral decomposition of the probability transfer matrix characterizing the nonequilibrium properties of the system. Finally, we checked the compatibility conditions, as well as the time-reversal symmetry conditions for short time steps. In many situations the methodology is consistent and provides a complete statistical description of the system. However, some discrepancies appear that deserve caution.

This study provided us with a systematic approach for reducing the number of pertinent macroscopical variables resulting into a manageable master equation.

ACKNOWLEDGMENTS

The authors acknowledge Prof. Enrique Tirapegui for bringing our attention to the coarse-graining methodology for reversible systems and for his participation in the early stages of this work. We also thank Fernando Mora for valuable comments. We would like to acknowledge both anonymous referees for a critical reading of the paper and some valuable remarks that resulted in an improvement of the original manuscript. In particular we are grateful for a remark regarding staggered invariants to which one of the referees drew our attention. F.U. thanks CONICYT (Chile) for financial support through Doctoral Scholarship No. 21140319. S.R. is grateful for a CONICYT Basal-CMM grant. Also, we thank Fondequip AIC-34.

[1] G. Nicolis and C. Nicolis, Phys. Rev. A **38**, 427 (1988).
[2] G. Nicolis, S. Martinez, and E. Tirapegui, Chaos Soliton. Fract. **1**, 25 (1991).
[3] G. Vichniac, Physica D **10**, 96 (1984).
[4] Y. Pomeau, J. Phys. A: Math. Gen. **17**, L415 (1984).
[5] H. Herrmann, J. Stat. Phys. **45**, 145 (1986).
[6] H. J. Herrmann, H. O. Carmesin, and D. Stauffer, J. Phys. A: Math. Gen. **20**, 4939 (1987).
[7] S. Takesue, Phys. Rev. Lett. **59**, 2499 (1987).
[8] E. Goles and S. Rica, Eur. Phys. J. D **62**, 127 (2011).
[9] S. Takesue, Complex Systems **9**, 149 (1995).
[10] L. Onsager, Phys. Rev. **65**, 117 (1944).
[11] C. N. Yang, Phys. Rev. **85**, 808 (1952).
[12] R. J. Glauber, J. Math. Phys. **4**, 294 (1963).
[13] F. Urbina, Equilibrium and non-equilibrium in a reversible and conservative cellular automaton, Ph.D. thesis, Universidad Adolfo Ibáñez, 2017.
[14] F. Urbina, M. Montalva, and S. Rica (unpublished).
[15] P. Grassberger, J. Stat. Phys. **45**, 27 (1986).
[16] Y. Pomeau, J. Phys. (Paris) **43**, 859 (1982).
[17] F. Urbina, S. Rica, and E. Tirapegui, Discontinuity Nonlinearity Complex. **4**, 19 (2015).